Design of a new turbine for OWC Wave Energy Converters: the DDT concept

García-Díaz, Manuel [(a)] *; Pereiras, Bruno [(a)]; Miguel-González, Celia [(a)]; Rodríguez, Laudino [(b)]; Fernández-Oro, Jesús [(a)]

[(a)] University of Oviedo, Energy Department, c/ Wifredo Ricart s/n, Gijón, Spain

[(b)] Centro Integrado de F.P. Mantenimiento y Servicios a la Producción de Langreo (C.I.F.P.M.S.P.), Ciudad Tecnológica e Industrial Valnalón, Hornos Altos S/N, 33930, La Felguera, Spain

* Corresponding author. Email address: garciadmanuel@uniovi.es

Abstract

At present time, the Oscillating Water Column (OWC) device seems to be one of the most promising wave energy technology. Recently, the Twin Turbines Configuration (TTC) has received attention because it is based on the use of unidirectional turbines which are much more efficient. Nevertheless, its main disadvantage with respect to classic OWC systems equipped with bidirectional turbines is the duplicity of equipment. To overcome this limitation, the Double Decker Turbine (DDT) concept is presented here as a new turbine which combines the best of both solutions, the TTC and the bidirectional turbine, in which the geometrical design of the DDT has been carried out based on a well-tested geometry taken from the bibliography. In addition, CFD modelling has been used to obtain an optimized DDT by means of a comparison between two new geometries for the outer turbine; while the inner turbine geometry has been already taken from the literature. Outer turbine has been further validated through experimental measurements of a manufactured prototype. Finally, a non-steady analysis of the proposed double turbine is carried out assuming sinusoidal flow conditions. Results demonstrate that the DDT concept can compete with the other alternatives, even envisaging high-performance characteristics to be developed in future works.

Keywords: Wave Energy, Oscillating Water Column, Double Decker Turbine, Twin Turbines Configuration, Axial Turbine

Nomenclature

$A_R = \pi*(r_{EX}^2-r_{IN}^2)$	Cross-Flow Area	[m^2]
c	Blade Chord	[m]
C_A	Dimensionless Input Coefficient	[-]
C_T	Dimensionless Torque Coefficient	[-]
D	Diameter	[m]
D_{REF}	Reference Diameter	[m]
N	Number of Blades	[-]
ΔP	Total to Static Pressure Difference	[Pa]
Q	Flow Rate	[$m^3\ s^{-1}$]

1	Q_{ExT}	Flow Rate across the ExT	[m^3 s^{-1}]
2	Q_{InT}	Flow Rate across the InT	[m^3 s^{-1}]
3	Q_{TOT}	Total Flow Rate across the DDT	[m^3 s^{-1}]
4	r_m	Mean Radius	[m]
5	r_{EX}	External Radius of the ExT	[m]
6	r_{IN}	Internal Radius of the InT	[m]
7	s	Solidity	[-]
8	T	Wave Period	[s]
9	t	Time	[s]
10	T_0	Torque	[N m]
11	T_{ExT}	Torque of the ExT	[N m]
12	T_{InT}	Torque of the InT	[N m]
13	T_{TOT}	Torque of the DDT	[N m]
14	u_R	Tangential Velocity at r_R	[m s^{-1}]
15	v_a	Velocity at the Cross-Flow Area	[m s^{-1}]
16	ω	Rotational Speed	[rad s^{-1}]
17	ρ	Air Density	[kg m^{-3}]
18	ϕ	Dimensionless Flow Coefficient	[-]
19	η	Total-to-Static Steady Efficiency	[-]
20	$\bar{\eta}_{NS}$	Non-Steady Efficiency	[-]
21	$\bar{\eta}_{Input}$	Input efficiency	[-]
22	$\bar{\eta}_{tg}$	Net efficiency of the DDT	[-]
23	Φ	Flow Coefficient of the Twin System	[-]
24	OWC	Oscillating Water Column	
25	TTC	Twin Turbines Configuration	
26	DDT	Double Decker Turbine	
27	GV	Guide Vanes	
28	PTO	Power-Take-Off	
29	InT	Internal Turbine	
30	ExT	External Turbine	

1. Introduction

Nowadays, Oscillating Water Column (OWC) seems to be one of the most promising wave energy technologies [1] [2]. Several OWC devices have been constructed mainly for research in the last decades and current trends predict more power plants to be installed in the next years [3]. The reason behind that success is that power transformation is made out of the sea, so the life span of the installations is enlarged [2], with a maintenance that is significantly easier in comparison to offshore wave energy devices [2]. Offshore devices maintenance must consider external conditions like wave height, operation needed time or weather, in order to plan the work. Also, typically a vessel is used as form transport to reach the power plant. This adds extra costs to the maintenance [4] and makes it more complex as is intended to do it only once a year [5].

Typically, OWC systems are composed of three parts: the OWC chamber, the PTO and the generator. The OWC chamber consists on a partially submerged chamber where the sea can enter and exit alternatively as the outside sea-level rises and falls. This oscillating motion of the water free-surface inside the chamber drives the air from the chamber towards the atmosphere (exhalation) or aspirates the air from the atmosphere to the chamber (inhalation) generating a bidirectional flow. The pneumatic energy is then exploited by the PTO to obtain mechanical energy, which is further transformed into electricity by a generator [6].

Over the years, the most convenient typology of the PTO has been discussed in many works [7][8]. Despite of the existence of others possibilities, the most widely installed configuration is based on a self-rectifying turbine, which rotates in the same direction regardless whence the flow is coming from [2]. This family of turbines are also known as “bidirectional” turbines. The Wells turbine, one of these self-rectifying turbines and the most selected one for OWC prototypes [7], was patented by A. Wells in 1976 [9]. It has a peak efficiency greater than other turbines but in a narrow range of flow coefficients, being this feature its main drawback [10]. Another bidirectional turbine is the impulse turbine, presented by Babintsev in 1980 [11], which has a peak efficiency lower than the Wells turbine, but maintaining relatively high values over a broader range of flow coefficients [2]. Both typologies have also a wide number of different sub-types, such as pitch controlled blades in case of the Wells turbine [2], turbines equipped with moving guide vanes or even multistage turbines. Apart from those two great families, the biradial turbine is another typology of bidirectional turbines that have been developed currently for OWC applications [12]. Alternatively, unidirectional turbines can also be used for this application if special designs are introduced to rectify the flow direction. Another possibility, firstly introduced by Jayashankar in 2009 [13], is the Twin Turbines Configuration (TTC), which consists in a OWC power plant equipped with two identical unidirectional turbines. Despite of preliminary studies reporting good results, there are no commercial installations mounting this type of system yet. Moreover, the TTC presents more operation problems than the bidirectional turbines, mostly related to the duplicity of the equipment required. Another problem is the reverse flow (flow that passes through the turbine when it is supposed to be working as a backflow preventer), which involves that only around 60% of the total flow generated by the OWC can be exploited [14]. However, combining the best features of both configurations, an optimal trade-off should be attained: having only one turbine, such as bidirectional solutions, but using them in an unidirectional fashion, which is much more efficient.

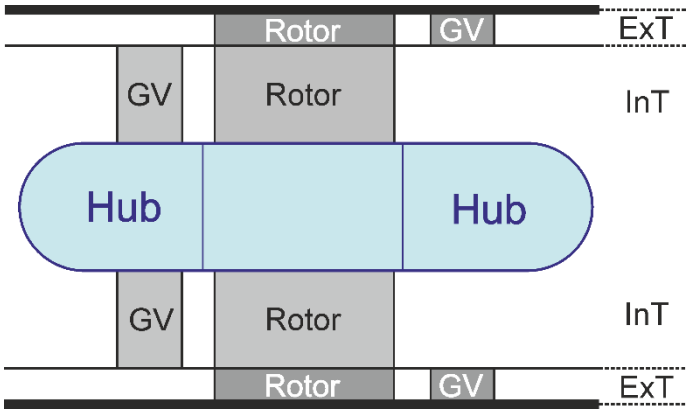

Figure 1 - Longitudinal scheme of the Double Decker Turbine

In this work, the authors present the Double Decker Turbine (DDT) concept [15], based on the Twin Turbines Configuration. DDT is a single turbomachine composed by two unidirectional turbines working in parallel with an outer turbine, which is called "External Turbine" (ExT), and an inner one called "Internal Turbine" (InT). Figure 1 shows a side view of the DDT, with both ExT and InT units composed of a single stage with guide vanes placed upstream of the rotor. In addition, note that both inner and outer rotors are joint in the same piece, rotating with the same direction and equal angular velocity. Each of the rotor rows exploits one of the flow directions with the addition of upstream guide vanes (as in a conventional unidirectional turbine) in order to increase the efficiency.

The performance of the DDT concept, which working principle is shown in Figure 2, is similar to the TTC [13] because it is also composed of two unidirectional turbines. When the air comes from the left, the major part of the flow passes through the InT, which it is working efficiently and extracting energy in the direct mode. This working condition is named as Internal Mode (IM). Conversely, when the air comes from the right, the InT blocks the flow (is now in reverse mode) and the ExT exploits the major part of the flow, establishing the so-called External Mode (EM). Previous works, despite of the drawbacks previously mentioned, show that unidirectional axial turbines in a TTC can reach greater performances than self-rectifying turbines in a conventional OWC. The aim of this work is to present the DDT and to prove that it can be as competitive as a TTC based on the same reference geometry. For this analysis, the performance curves for both InT and ExT units are obtained separately and finally combined to emulate the non-steady behaviour of the DDT as a whole.

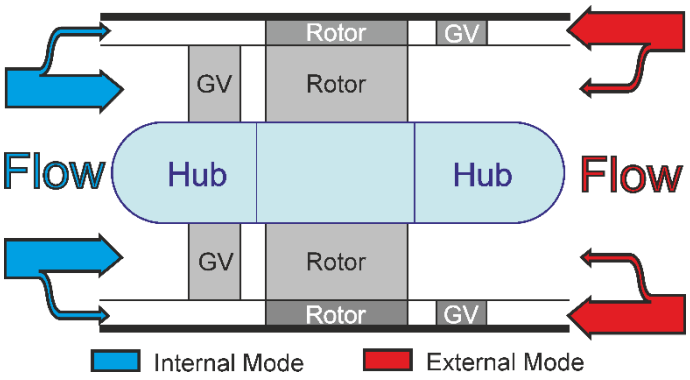

Figure 2 - Flow distribution and operating modes of the Double Decker Turbine

2. Design of the turbine

Although the DDT is composed of two unidirectional, geometrically different, turbines, it is desirable to maintain similar performance curves of both units, in order to ensure that the whole DDT has a near-symmetric behaviour between both flow directions. Eventually, a mismatch in the pressure drop curves may cause an unequal flow distribution that would increase the output in one flow direction while decreasing the performance in the other flow direction.

This first version of the DDT was based on the turbine presented in [14], which offers a greater performance than previous versions [16], keeping the rotational velocity unchanged (ω = 375 rpm). In particular, the InT of the DDT is defined exactly with the same geometry [14], whose main geometric parameters are shown in Figure 3. The number of blades (30) and vanes (24) has been also preserved, with identical blade profiles, so its performance curves are those shown in [14]. On the other hand, with the objective to maintain similar axial flow velocities in both turbines, the ExT is designed to have the same pass-through area than the InT, thus leading to a blade span shorter than in the InT.

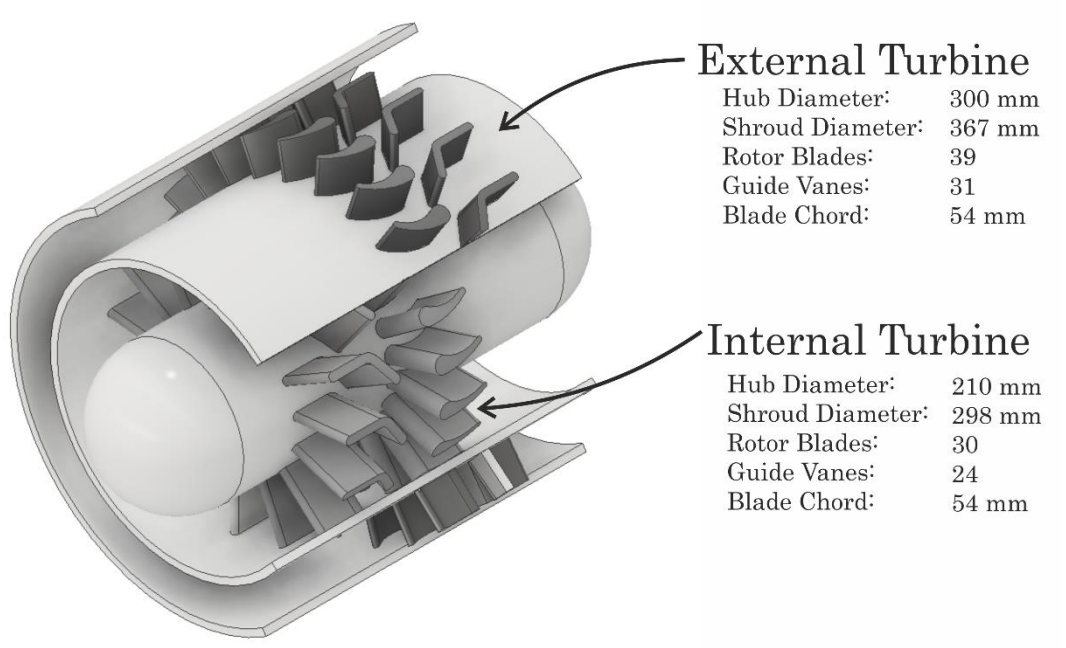

Figure 3 - 3D view of the DDT with its basic geometric parameters

Two different geometries were tested for the ExT, in order to obtain a performance curve similar to the one of the InT, especially in terms of C_A. As a first attempt, the same blade profiles used for the InT were adopted for the ExT, mainly characterized by an outlet blade angle of 60 deg (named as "original" blade shape, see figure 4). However, the outlet flow presented a significant axial deviation as a consequence of the higher blade velocity (associated to the higher radius of the external midspan). To overcome this problem, it was decided to increase the blade flow deflection, modifying the geometry with an outlet blade angle of 55 deg ("modified" blade shape, see figure 4). This change in the trailing edge resulted in an axial flow at the rotor exit for the design point and a further increase of the maximum efficiency of the ExT. In fact, the correction of that blade angle mismatch allowed the more efficient performance of the ExT, as expected from its smaller hub-to-tip ratio, according to the scientific literature ([17, Chapter 2] [18, Chapter 4]): A lower blade span in a turbine reduces

three-dimensional effects and makes all the blade sections work similar to the mid-span section, closing the overall performance to the baseline design. All these features are discussed later in detail in Figure 13. The rest geometrical parameters of both InT and ExT turbines have been kept unchanged. In particular, the guide vanes design, the blade LE angle as well as the solidity were preserved. Note that the solidity, defined as the number of blades multiplied by the chord length of the blade and divided by the mean radius of the blade row (Equation 1), gives a value of 6.4 in both turbine rotors.

$$s = \frac{Nc}{r_m} \tag{1}$$

The performance curves of both "original" and "modified" blade shapes in the ExT rotor are obtained using a commercial CFD code. In addition, they have been compared to the performance curve of the InT to check that a near-equal flow distribution in both flow directions is ensured with the improved modifications. The results are presented later in sub-section 6.2.

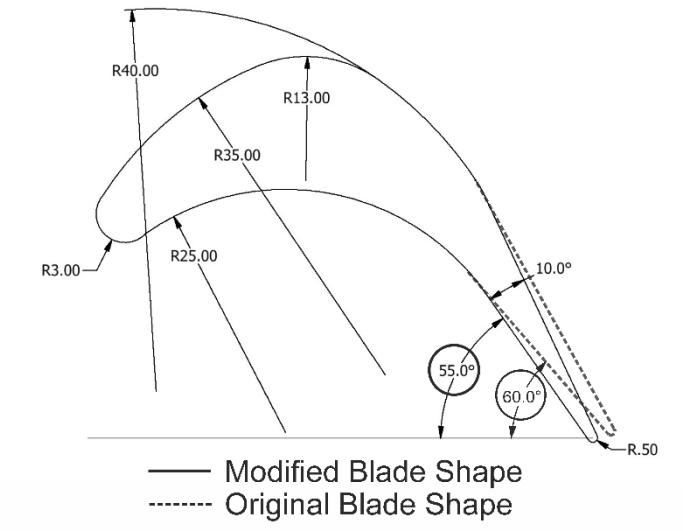

Figure 4 - Modified and original blade shapes of the ExT, with different trailing edge angles

3. Dimensionless Coefficients

The turbine performance is analysed in terms of the classical dimensionless coefficients for OWC turbines. Since InT and ExT have different mean radius, the coefficients are built using the same reference diameter, D_{REF} = 0.298 m, which corresponds to the shroud diameter of the InT. This allows to provide an overall performance curve of the DDT as a whole.

In addition, the use of a reference diameter in the classic, non-dimensional coefficient, also guarantees a correct comparison of the turbine units separately. Otherwise, the same pressure drop would be incorrectly normalized, leading to artificial re-scalings of the results. Hence, the coefficients were defined as:

$$\phi = \frac{4\,Q}{\pi\,D_{REF}^3\,\omega} \tag{2}$$

$$C_T = \frac{T_0}{\frac{1}{2}\rho(v_a^2 + u_R^2)A_R r_{REF}} \tag{3}$$

$$C_A = \frac{\Delta P}{\frac{1}{2}\rho(v_a^2 + u_R^2)} \tag{4}$$

$$\eta = \frac{C_T}{C_A \phi} \tag{5}$$

where the meaning of the different variables can be found in the nomenclature section.

Once the performance curves are obtained, a non-steady analysis is conducted to assess the performance of the DDT under sinusoidal flow conditions, being the calculations based on the steady performance of each turbine. The formulation can be seen in equations 6 to 11, applied for different flow coefficients, Φ. Applications of this method can be seen in [16] [19]. This formulation had to be rewritten to adapt this new topology to the present DDT design, considering also the presence of two turbines.

$$\Phi = \Phi_{MAX}\, sin\left(\frac{2\pi t}{T}\right) \tag{6}$$

Where Φ is the instantaneous total flow coefficient, Φ_{MAX} is the amplitude flow coefficient, T is the wave period (10 seconds for this analysis) and t is time.

$$\bar{\eta}_{NS} = \frac{{}^1\!/_T \int_0^T \omega\, T_{TOT}\, dt}{{}^1\!/_T \int_0^T \Delta P_t\, Q_{TOT}\, dt} \tag{7}$$

As the DDT has an implicit non-symmetric behaviour in both flow directions, the integral can be decomposed in two parts:

$$\bar{\eta}_{NS} = \underbrace{\frac{{}^1\!/_T \int_0^{T/2} \omega\, (T_{InT} + T_{ExT})\, dt}{{}^1\!/_T \int_0^T \Delta P_t\, (Q_{InT} + Q_{ExT})\, dt}}_{IM} + \underbrace{\frac{{}^1\!/_T \int_{T/2}^T \omega\, (T_{ExT} + T_{InT})\, dt}{{}^1\!/_T \int_0^T \Delta P_t\, (Q_{InT} + Q_{ExT})\, dt}}_{EM} \tag{8}$$

According to Figure 2, during the first part of the wave period in the IM, the InT is producing energy whereas ExT is blocking the flow. When the flow direction is reversed during EM, in the second part of the wave period, both InT and ExT units switch their roles. Note that, during each performance mode, the torque produced by each turbine could be eventually changing its sign, according to the working mode of the DDT. Therefore, each part of the equation has to be decomposed according to:

$$\underbrace{\frac{{}^1\!/_T \int_0^{T/2} \omega\, (T_{InT} + T_{ExT})\, dt}{{}^1\!/_T \int_0^T \Delta P_t\, (Q_{InT} + Q_{ExT})\, dt}}_{IM} = \underbrace{\frac{{}^1\!/_T \int_0^{T/2} \Delta P_t\, Q_{InT}\, dt}{{}^1\!/_T \int_0^T \Delta P_t\, (Q_{InT} + Q_{ExT})\, dt}}_{\bar{\eta}_{input}^{IM}} \underbrace{\frac{{}^1\!/_T \int_0^{T/2} \omega\, (T_{InT} + T_{ExT})\, dt}{{}^1\!/_T \int_0^{T/2} \Delta P_t\, Q_{InT}\, dt}}_{\bar{\eta}_{tg}^{IM}} \tag{9}$$

$$\underbrace{\frac{{}^1\!/_T \int_{T/2}^T \omega\, (T_{ExT} + T_{InT})\, dt}{{}^1\!/_T \int_0^T \Delta P_t\, (Q_{InT} + Q_{ExT})\, dt}}_{EM} = \underbrace{\frac{{}^1\!/_T \int_{T/2}^T \Delta P_t\, Q_{ExT}\, dt}{{}^1\!/_T \int_0^T \Delta P_t\, (Q_{InT} + Q_{ExT})\, dt}}_{\bar{\eta}_{input}^{EM}} \underbrace{\frac{{}^1\!/_T \int_{T/2}^T \omega\, (T_{ExT} + T_{InT})\, dt}{{}^1\!/_T \int_{T/2}^T \Delta P_t\, Q_{ExT}\, dt}}_{\bar{\eta}_{tg}^{EM}} \tag{10}$$

$$\bar{\eta}_{NS} = \bar{\eta}_{input}^{IM}\,\bar{\eta}_{tg}^{IM} + \bar{\eta}_{input}^{EM}\bar{\eta}_{tg}^{EM} \quad (11)$$

4. Numerical Model

The InT was previously analysed by the authors using a well-validated CFD model [14], so those results were assumed to be reliable as a starting point for this work. Taking advantage of such numerical methodology, a new CFD model has been developed and applied for the ExT unit of the DDT design presented.

The numerical analysis was made with the commercial software ANSYS Fluent v16.2, which uses the finite volume method to solve the Navier-Stokes equations in its incompressible form using a segregated solver [14] [20]. Moreover, an unsteady Reynolds-averaged Navier-Stokes equations approach (URANS) was adopted to guarantee a full consideration of the interaction effects between moving and fixed rows in the DDT stage. The domain simulated consists on one sixth of the full annulus of the ExT, in order to save CPU time and promote the refinement of the mesh in some areas. To meet the periodicity condition for the turbine, a slight tangential modification had to be introduced, reducing the number of guide vanes from 31 to 30 and the number of rotor blades from 39 to 36.

The mesh was built using ANSYS TurboGrid, which is a software specifically design to create high quality hexaedrical meshes for turbomachinery applications. Figure 5 shows the blocking strategy used in TurboGrid for both rotor blades and guide vanes to obtain 2D mappeable sub-domains. The mapped mesh generated is then extruded along the span direction to create the 3D structured mesh. The overall quality of the mesh is shown in Figure 6 in terms of Equiangle Skewness, revealing that most of the elements are beyond the 0.8 value and that the mesh quality is optimal for CFD proposals. Special attention was paid to the boundary layer mesh near the walls, with typical distances of the first grid point to the wall around 0.0075 mm.

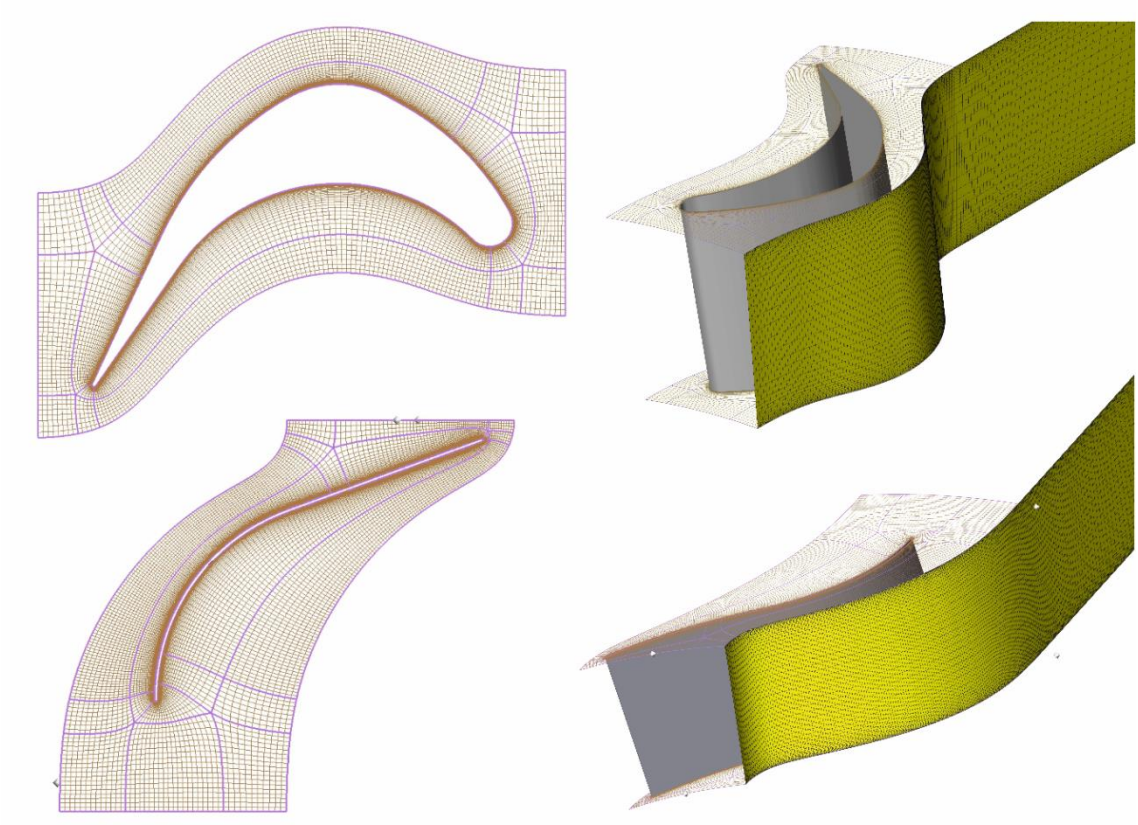

Figure 5 - Detail of the mesh in the rotor blades and guide vanes of the DDT

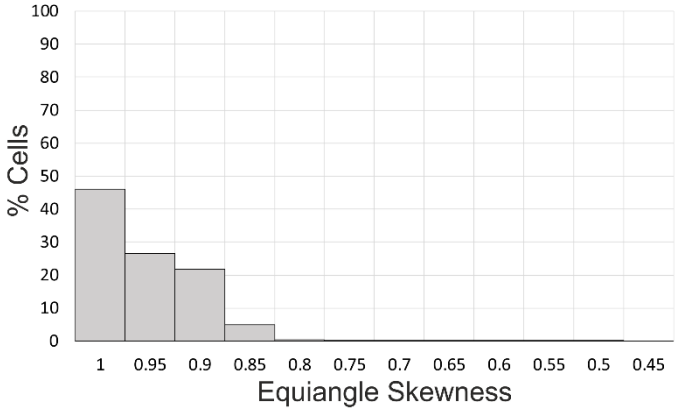

Figure 6 - Mesh quality in terms of Equiangle Skewness (Value of 1 corresponds to a perfect hexaedrical cell)

Not only the quality of the mesh is a significant concern, but also the total number of grid elements is of paramount importance to obtain accurate, converged results in the model. For that purpose, an additional mesh sensitivity analysis was conducted for this model using four different meshes with 1.8, 3.2, 6.1 and 8.5 million cells respectively. The torque and input coefficients, normalized with the maximum values of the coarser mesh, are represented against mesh size in Figure 7. In order to ensure maximum differences below 1% in all the main coefficients, the finer mesh was finally chosen to carry out the bulk set of simulations. This final mesh density, with approximately 8.5 million hexaedrical cells, takes into account special refinements close to the walls in order to use a more precise, high-order near-wall treatment scheme.

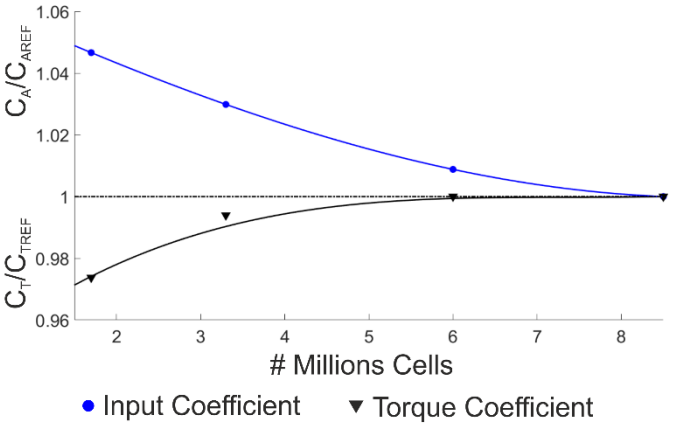

Figure 7 - Mesh sensibility analysis, with the reference value taken from the coarser mesh size

With respect to the turbulence modelling, a robust, two-equation k-ε Realizable model was selected for the simulations [14] [20], using non-equilibrium wall functions in correspondence to the y^+ values slightly larger than 1 [21] in most of the solid walls.

The boundary conditions of the simulations, shown in Figure 8, include a velocity-inlet, a pressure-outlet (assuming atmospheric conditions), the lateral periodicities and the interface in the interrow region upstream of the rotor to allow the use of the sliding mesh technique for a full unsteady simulation. Computations were carried out with SIMPLE scheme for the pressure- velocity coupling, a third-order discretization for pressure and momentum and second order for the transient formulation, turbulent kinetic energy and turbulent dissipation rate. Residuals were set to 10^{-5} and the time step size was fixed to 10^{-4} s, which corresponds to 444 time steps per blade event, taking 20 iterations per time step to converge. With these settings each simulation lasted about 1 day to complete 5 rotating cycles of the domain in a cluster composed of computers equipped with 32Gb and Intel i7-6800K processors.

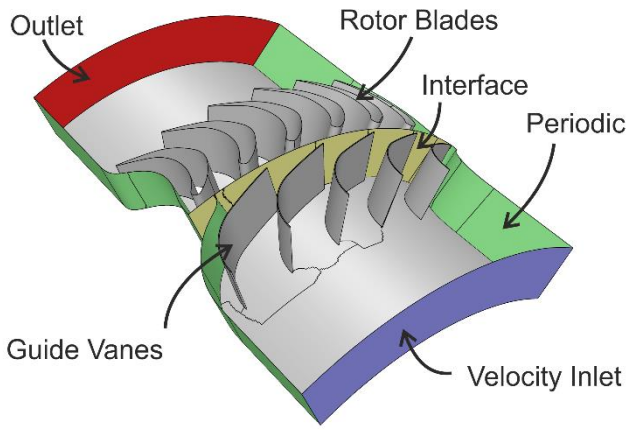

Figure 8 - Boundary Conditions of the simulation

Finally, note that since the time scales within the turbine stages (i.e., the blade passing frequency of the ExT rotor is 243.75 Hz) are three orders of magnitude lower than the global fluctuations in the OWC system (the incoming waves at the boundaries with a typical frequency of 0.1 Hz), it can be perfectly assumed that the turbine works under quasi-steady boundary conditions in regard to the wave time scales.

5. Test Rig

To ensure the reliability of the numerical data, an experimental model of the ExT was constructed and tested in direct mode, when the turbine is exploiting the flow. The geometry chosen was the modified blade shape, corresponding to a 55 deg outlet angle. The experimental tests were carried out in a test rig built for this work (Figure 9). The turbine (6 and 7, Figure 9) is connected to a DC motor (9, Figure 9), which nominal values are 36V, 2800rpm and 250W. In order to measure in a whole range of flow coefficients, the DC motor can work as motor or generator. For low flow coefficients, the turbine has to rotate at very high speed, so the DC motor is connected to a power supply (12, Figure 9). On the other hand, when a high flow coefficient is to be measured, the turbine rotates at low speed and the DC motor is then connected to a variable resistance, which is within the range [4, 50] Ω. In both cases, voltage and current are measured to calculate the energy consumed/generated by the turbine.

The test rig is equipped with two manometers (4 and 5, Figure 9), which measure the pressure difference in the Venturi meter (3, Figure 9) and the pressure difference across the turbine. Also, a tachometer (8, Figure 9) measures the rotational speed and two multimeters (10 and 11, Figure 9) measure voltage and current inputs or outputs of the motor. The fan (1, Figure 9) is equipped with a frequency converter (Siemens Sinamics V20) in order to change the flow rate across the turbine. The tube (2, Figure 9) has an enlargement of 304 mm diameter where the turbine (300 mm shroud external diameter) is placed, thus a gap of 2 mm allows the turbine to rotate without friction. Especial attention was paid on avoiding any air leaking through the interrow clearance.

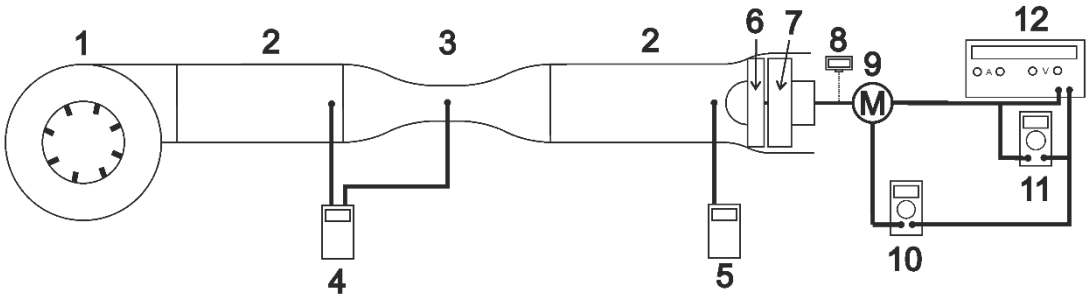

Pos.	Denomination	Pos.	Denomination
1	Fan Rosenberg ERND 355-4	7	Rotor
2	Tube D=300 mm	8	Tachometer TDM20X
3	Venturi Meter	9	Motor HappyMotors MY1015
4	Sensirion SDP800-125Pa	10	Multimeter FLUKE 117
5	Manometer KIMO CP 210	11	Multimeter FLUKE 115
6	Stator	12	Power Supply EA-PS 8360-10T

Figure 9 - Test rig and equipment

The accuracies of all the measurement equipment used are collected in Table 1.

Table 1 - Accuracy of the measurement equipment

Sensirion SDP800-125Pa	Pressure	3% + 0.08 Pa
Manometer KIMO CP210	Pressure	0.5% + 2 Pa
Tachometer TDM20X	Rotational speed	1 rpm

Multimeter FLUKE 115	Voltage	0.5% + 0.02 V
Multimeter FLUKE 117	Intensity	1% + 0.003 A

The experimental model of the turbine was made in a 3D printer in PolyLactic Acid (PLA). The 3D printer used is a "The Beast v1.2", manufactured by Cultivate 3D. It is a large format printer which can build volumes up to 470x435x670 mm, allowing to print relatively large parts. For this work, a nozzle of 0.3 mm and a layer height of 0.1 mm were used. In Figure 10, a photograph of a blade shows the quality of the surface roughness given by the printer. The Venturi meter, calibrated following the standards [22], was designed and built in PLA with the 3D printer by the authors.

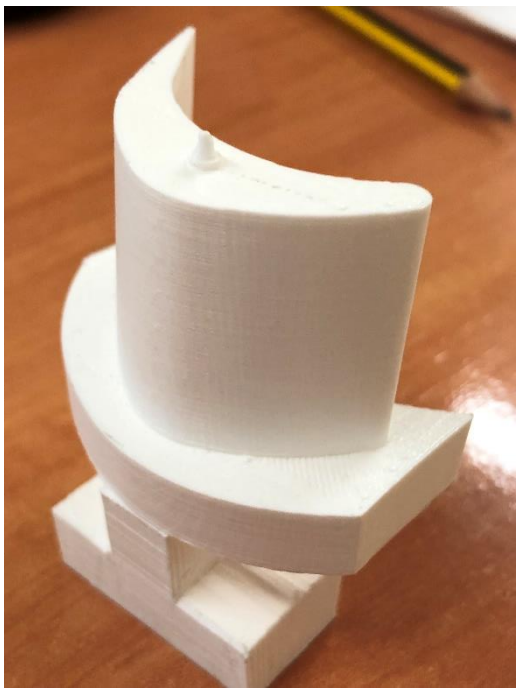

Figure 10 - Photograph of one blade. Detail of the surface roughness

Figure 11 shows an exploding view of the mechanical design of the tested turbine (ExT). All the printed parts of the experimental model were glued or assembled together. The rotor was designed with a slotted hub (8, Figure 11) [23][24] and 36 single rotor blades (6, Figure 11) were fixed in the slotted hub and enclosed by a counterpart (5, Figure 11). The stator was fixed to the tube (2, Figure 9) and internally to the support part (3, Figure 11). The alignment and dynamic response of the shaft (9, Figure 11) at the nose (1, Figure 11) is guaranteed by an internal bearing (2, Figure 11).

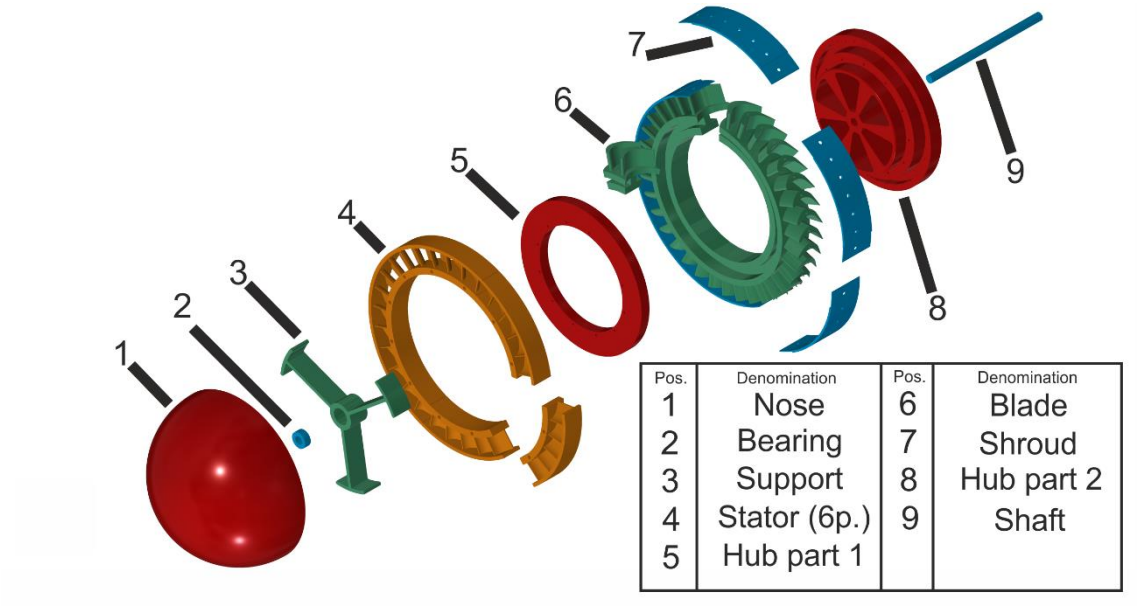

Pos.	Denomination	Pos.	Denomination
1	Nose	6	Blade
2	Bearing	7	Shroud
3	Support	8	Hub part 2
4	Stator (6p.)	9	Shaft
5	Hub part 1		

Figure 11 – Exploding view of the experimental model of the turbine

The electrical and mechanical losses of the turbine were assessed in a first step using the power supply, the multimeters and the tachometer, following a similar methodology to that previously used by the authors [19] [25]. The power consumption of the turbine rotating at stable speed was analysed to calculate both electrical and mechanical losses. Since the DC motor has a known electric resistance of 0.9 Ω, the electrical and mechanical losses can be decoupled afterwards. Note that the pumping effect caused by the turbine was considered negligible with respect to electrical and mechanical losses.

6. Results and discussion

6.1. Validation

Firstly, CFD and experimental data are compared in Figure 12 for validation purposes. In the top plot, the distribution of the pressure coefficient as a function of the flow coefficient is shown, revealing a good agreement between numerical (solid markers) and experimental (blank markers) data. The torque coefficient from the CFD model (bottom plot) predicts also pretty well the trend of the experimental curve. In all the coefficients, the discrepancies are higher as the flow coefficient is increased. The maximum disparity between the numerical and the experimental data is around 19%, being located at high flow coefficients (*Ø=1.5)* and only at the dimensionless input coefficient, which it is considered acceptable to validate the CFD model for the present work.

It must be pointed out that the experimental results in the plots present significant uncertainties associated to the measurement instruments. The final uncertainty of the experimental values has been calculated using the theory for uncertainty transmission defined by Kline [26]. The uncertainty of the measurements is within the 3% and 4% for the *Ø*, 1.9% and 6.5% for C_A and 1.8% and 7% for the C_T.

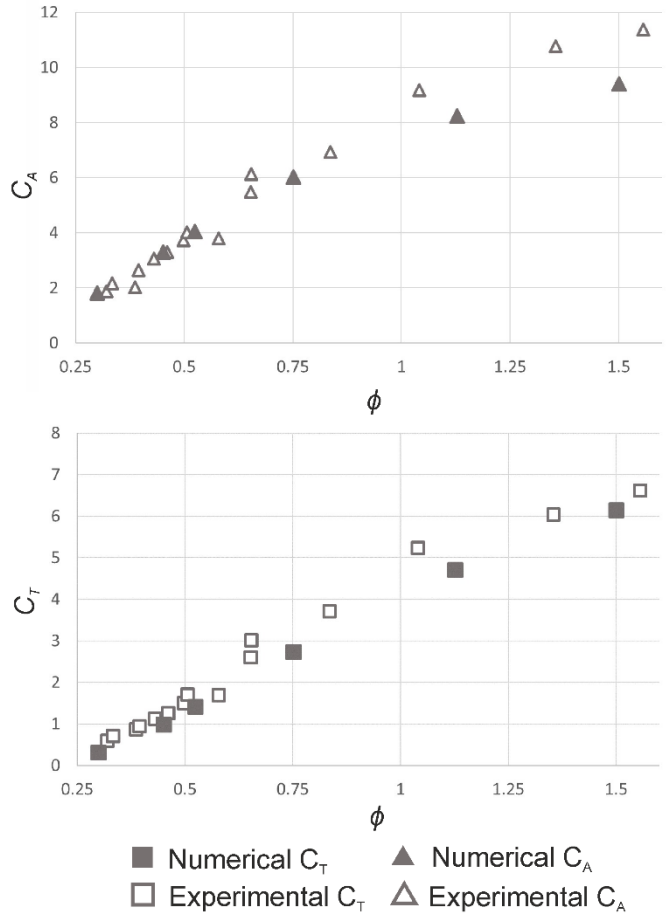

Figure 12 – Comparison of numerical (solid markers) and experimental data (blank markers) for the ExT unit with the modified blade shape

6.2. Analysis of the ExT geometries

After validation, the CFD results for both ExT and InT units are compared in Figure 13. In addition, the results from the original blade shape and the modified one have been included for completeness. The comparison is performed for the torque coefficient (C_T in the top plot), the pressure coefficient (C_A in the middle plot) and the total-to-static efficiency (η in the bottom plot). Data of the performance curves of the InT was taken from previous published results in Pereiras [14], while results for both ExT geometries are given by the CFD model. As expected from kinematic considerations (velocity triangles), the pressure coefficient curve in direct mode of the modified blade shape matches better with the curve of the InT.

Note that the torque is negative for the InT and the ExT in reverse mode when they are working as flow preventers. Consequently, this negative torque is to be subtracted from the torque of the turbine exploiting the flow in the following non-steady analysis done in subsection 6.3 (equations 8 and 9). It is remarkable that the ExT has a lower negative torque than the InT, leading to an unexpected efficiency improvement of the DDT during the IM.

Regarding the turbines efficiencies, the ExT has slightly higher values than the InT for the whole range of flow coefficients as a consequence of its lower hub-to-tip ratio and its associated lower flow deflection, as explained earlier (see also [17, Chapter 2]. Basically, three dimensional effects are reduced in the ExT, with lower centrifugal forces due to the higher mean radius of the ExT, which leads to an enhancement of the efficiency and a lower level of losses [18, Chapter 4].

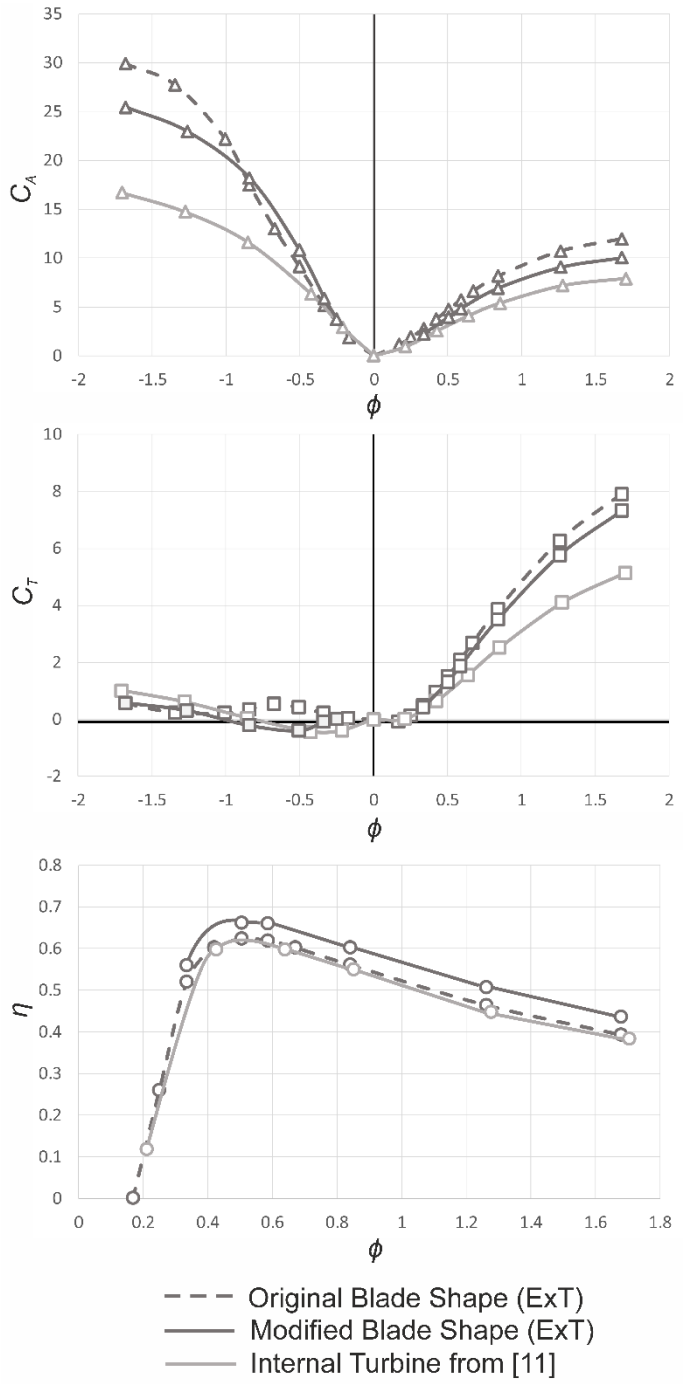

Figure 13 Numerical comparison of the Dimensionless Coefficients for the InT and Ext geometries analyzed

In summary, the presented results justify the selection of the modified blade shape for the ExT, while maintaining the geometry taken from [14] for the InT. This configuration will offer an enhanced flow rate distribution and, therefore, a better global performance. Future works should focus on making the performance of both turbines as similar as possible, looking for further optimization of the flow distribution and the efficiency of both InT and ExT units.

6.3. Non-Steady Analysis with CFD data

In this section, the performance curve from the CFD modelling, resolved unsteadily (for the turbine rotation) but with stationary boundary conditions, is used as input data to estimate the

non-steady response of the whole DDT when the wave conditions are introduced in the analysis of the OWC device. This classic methodology has been successfully employed in the literature in previous works [13] [14] [19], taking advantage of the spectral gap between the turbine time scales and the temporal cycles of the waves, as discussed at the end of section 4.

For the analysis of the DDT under non steady conditions, a sine wave input coming from the OWC chamber is assumed. Hence, different working points can be analysed changing the amplitude of this sinusoidal input.

Taking into account that the pressure difference across both turbines is the same, the instantaneous flow coefficient of the DDT is computed as the sum of the individual flow coefficients of both InT and ExT. This allows to obtain the overall flow rate distribution, torque and efficiency of the DDT in the temporal domain. Notice that in other works, where a TTC was analysed using the same methodology [13] [14] [19], the first and second hemicycle of the sinusoidal flow were found to be symmetric. In the present case, the DDT behaviour as bidirectional turbine is not symmetric, so the positive part corresponds to the IM and the negative part corresponds to the EM which leads to a mismatch between both modes.

Figure 14 shows the temporal response of the DDT during the wave cycle for a maximum flow coefficient of $\phi_{MAX}=0.5$, corresponding to almost the best efficiency point of the turbine. Note that sea waves with higher (or lower) amplitudes would generate higher (or lower) peak flow rates accordingly. The IM hemicycle presents a better distribution of the flow rate, maximizing the direct mode flow with respect to the reverse one.

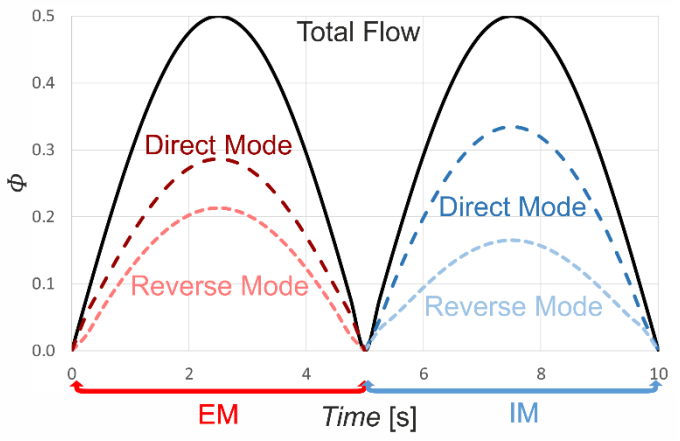

Figure 14 - Flow distribution for $\Phi_{MAX}=0.5$

Finally, the averaged non-steady performance of the turbine for a typical range of maximum flow coefficients (from 0 to 2.5) is represented in Figure 15. In addition, the same results for a twin turbines system (taken from [14]) and a classical bidirectional impulse turbine (taken from [27]) have been also included to compare the overall efficiency from different solutions. It is observed that the peak efficiency of the DDT is slightly higher than the maximum values of its competitors. In addition, and taking into account that the geometry can be further improved by optimizing each turbine separately, the authors consider that the DDT can be a real candidate for OWC devices like twin turbines configurations or self-rectifying turbines without moving parts. The figure also advices that the DDT performance is lower for higher flow coefficients with respect to the other systems. This fact can be explained by the curves of the InT and ExT, in which the mismatch is greater for high flow coefficients, leading to an unequal flow distribution and a reduction of the non-steady performance.

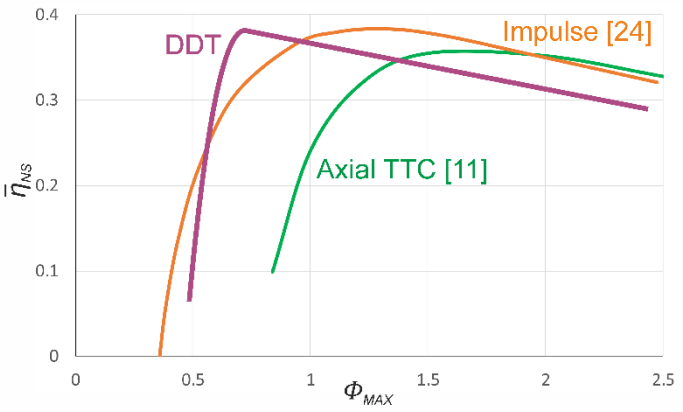

Figure 15 - Non-steady performance of the DDT. Comparison with others solutions from the bibliography: an impulse bidirectional turbine [27] *and a TTC with axial turbines* [14]

7. Conclusions

This work presents a new turbine, the DDT concept, specifically designed to work in OWC wave energy converters. This turbine tries to integrate the advantages of bidirectional turbines and twin turbines systems in a unique machine: A single turbine composed of two unidirectional turbines. The main advantage of this new concept is its compactness. The DDT avoids the duplicity of equipment of typical twin turbines systems, which in turn compromises its economic viability, by combining the whole TTC into a single turbine with only one generator. At the same time, the construction of the OWC chamber is also less complex.

The performance of the DDT has been assessed analytically by compounding the performance of both unidirectional turbines, named as InT and ExT units. The inner unit has been taken from the bibliography, whereas two different geometries were tested for the external part. Precisely, the performance of the geometries for the external part was calculated using a URANS-based CFD simulation that was experimentally validated with steady tests of the internal turbine.

The CFD results from these simulations were further employed as input data for a non-steady numerical analysis of the DDT in response to typical sinusoidal flow conditions of the sea waves within the OWC chamber. The non-steady performance of the design has revealed that averaged non-steady efficiencies of the DDT are well within the typical ranges provided by TTCs or self-rectifying turbines. Peak efficiencies of roughly a 40% are perfectly attained at the best efficiency point.

It is concluded that DDT seems to be competitive with the other alternatives of turbines, non-equipped with moving blades/vanes or check valves, reaching a maximum non-steady efficiency of 38%, similar to other solutions found in the bibliography.

8. Acknowledgements

Manuel García is supported by the Spanish ‘‘Ministerio de Educación, Cultura y Deporte’’ within the ‘‘FPU’’ Program (grant number FPU15/04375).

Celia Miguel is supported by the Spanish “Ministerio de Educación Cultura y Deporte” within the “Doctorados Industriales” Program (grant number DI-17-09596)

9. References

[1] M. Melikoglu, Current status and future of ocean energy sources: A global review, Ocean Eng. 148 (2018) 563–573. doi:10.1016/j.oceaneng.2017.11.045.

[2] A.F.O. Falcão, J.C.C. Henriques, Oscillating-water-column wave energy converters and air turbines: A review, Renew. Energy. 85 (2016) 1391–1424. doi:10.1016/j.renene.2015.07.086.

[3] A. Parsons, R. Gruet, Ocean Energy: Key Trends and Statistics 2018, (2018).

[4] S. Astariz, G. Iglesias, The economics of wave energy: A review, Renew. Sustain. Energy Rev. 45 (2015) 397–408. doi:10.1016/J.RSER.2015.01.061.

[5] M. O'connor, T. Lewis, G. Dalton, Weather window analysis of Irish and portuguese wave data with relevance to operations and maintenance of marine renewables, Proc. Int. Conf. Offshore Mech. Arct. Eng. - OMAE. 8 (2013) 1–13. doi:10.1115/OMAE2013-11125.

[6] I. López, J. Andreu, S. Ceballos, I. Martínez De Alegría, I. Kortabarria, Review of wave energy technologies and the necessary power-equipment, Renew. Sustain. Energy Rev. 27 (2013) 413–434. doi:10.1016/j.rser.2013.07.009.

[7] A. Sayigh, ed., Comprehensive Renewable Energy, First Edit, 2012. doi:10.5860/choice.50-3873.

[8] T. Setoguchi, M. Takao, Current status of self rectifying air turbines for wave energy conversion, Energy Convers. Manag. 47 (2006) 2382–2396. doi:10.1016/j.enconman.2005.11.013.

[9] A.A. Wells, Fluid driven rotary transducer, British Patent Spec. No. 1595700, 1976.

[10] P.M. Kumar, P. Halder, A. Husain, A. Samad, Performance enhancement of Wells turbine: Combined radiused edge blade tip, static extended trailing edge, and variable thickness modifications, Ocean Eng. 185 (2019) 47–58. doi:10.1016/j.oceaneng.2019.05.041.

[11] I.A. Babintsev, Apparatus for Converting Sea Wave Energy Into Electrical Energy, 96 (1980) 62–66. doi:US005485919A.

[12] A.F.O. Falcão, L.M.C. Gato, J.C.C. Henriques, J.E. Borges, B. Pereiras, F. Castro, A novel twin-rotor radial-inflow air turbine for oscillating-water-column wave energy converters, Energy. 93 (2015) 2116–2125. doi:10.1016/j.energy.2015.10.046.

[13] V. Jayashankar, S. Anand, T. Geetha, S. Santhakumar, V. Jagadeesh Kumar, M. Ravindran, T. Setoguchi, M. Takao, K. Toyota, S. Nagata, A twin unidirectional impulse turbine topology for OWC based wave energy plants, Renew. Energy. 34 (2009) 692–698. doi:10.1016/j.renene.2008.05.028.

[14] B. Pereiras, P. Valdez, F. Castro, Numerical analysis of a unidirectional axial turbine for twin turbine configuration, Appl. Ocean Res. 47 (2014) 1–8. doi:10.1016/j.apor.2014.03.003.

[15] M. García Díaz, L. Rodriguez, B. Pereiras, Turbina para aprovechamiento de flujo bidireccional, 2 729 207, 2018.

[16] M. Takao, A. Takami, S. Okuhara, T. Setoguchi, A twin unidirectional impulse turbine for wave energy conversion, J. Therm. Sci. 20 (2011) 394–397. doi:10.1007/s11630-011-

0486-1.

[17] B. Lakshminarayana, Fluid Dynamics and Heat Transfer of Turbomachinery, 1996.

[18] C.A. Dixon S.L.; Hall, Fluid Mechanics and Thermodynamics of Turbomachinery, n.d.

[19] L. Rodríguez, B. Pereiras, J. Fernández-Oro, F. Castro, Viability of unidirectional radial turbines for twin-turbine configuration of OWC wave energy converters, Ocean Eng. 154 (2018) 288–297. doi:10.1016/j.oceaneng.2018.02.010.

[20] A. Thakker, T.S. Dhanasekaran, Computed effects of tip clearance on performance of impulse turbine for wave energy conversion, Renew. Energy. 29 (2004) 529–547. doi:10.1016/j.renene.2003.09.007.

[21] Y. Cui, Z. Liu, X. Zhang, C. Xu, Review of CFD studies on axial-flow self-rectifying turbines for OWC wave energy conversion, Ocean Eng. 175 (2019) 80–102. doi:10.1016/j.oceaneng.2019.01.040.

[22] UNE, UNE 77225 “Emisiones de fuentes estacionarias. Medidas de velocidad y caudal volumétrico de corrientes de gases en conductos,” (2000).

[23] A. Thakker, J. Jarvis, M. Buggy, A. Sahed, 3DCAD conceptual design of the next-generation impulse turbine using the Pugh decision-matrix, Mater. Des. 30 (2009) 2676–2684. doi:10.1016/j.matdes.2008.10.011.

[24] C. Soares, Gas Turbine Major Components and Modules, 2008. doi:10.1016/b978-075067969-5.50009-0.

[25] L. Rodríguez, B. Pereiras, J. Fernández-Oro, F. Castro, Optimization and experimental tests of a centrifugal turbine for an owc device equipped with a twin turbines configuration, Energy. (2019). doi:10.1016/j.energy.2019.01.029.

[26] S.J. Kline, F.A. McClintock, Describing Uncertainties in Single-Sample Experiments, Mech. Eng. (1953).

[27] H. Maeda, S. Santhakumar, T. Setoguchi, M. Takao, Y. Kinoue, K. Kaneko, Performance of an impulse turbine with fixed guide vanes for wave power conversion, Renew. Energy. 17 (1999) 533–547. doi:10.1016/S0960-1481(98)00771-X.